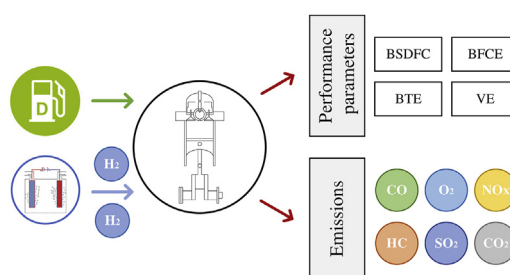Research article

# Experimental assessment of performance and emissions for hydrogen-diesel dual fuel operation in a low displacement compression ignition engine

L. Estrada [a], E. Moreno [a], A. Gonzalez-Quiroga [b], A. Bula [b], J. Duarte-Forero [a,*]

[a] KAI Research Unit, Department of Mechanical Engineering, Universidad del Atlántico, Carrera 30 Número 8–49, Puerto Colombia, Barranquilla, Colombia
[b] UREMA Research Unit, Department of Mechanical Engineering, Universidad del Norte, Barranquilla, Colombia

HIGHLIGHTS

- Performance and emissions for engine speeds of 3000 and 3600 rpm and torque levels of 3 and 7 Nm.
- $H_2$ for diesel substitution was generated in an in-house designed and built alkaline cell.
- Brake Fuel Conversion Efficiency decreases, the impact depending on engine speed and torque.
- Markedly lower CO and $CO_2$ emissions than neat diesel for the same power output but higher $NO_x$.

GRAPHICAL ABSTRACT

ABSTRACT

The combustion of pure $H_2$ in engines is still troublesome, needing further research and development. Using $H_2$ and diesel in a dual-fuel compression ignition engine appears as a more feasible approach. Here we report an experimental assessment of performance and emissions for a single-cylinder, four-stroke, air-cooled compression ignition engine operating with neat diesel and $H_2$-diesel dual-fuel. Previous studies typically show the performance and emissions for a specific operation condition (*i.e.* a fixed engine speed and torque) or a limited operating range. Our experiments covered engine speeds of 3000 and 3600 rpm and torque levels of 3 and 7 Nm. An in-house designed and built alkaline cell generated the $H_2$ used for the partial substitution of diesel. Compared with neat diesel, the results indicate that adding $H_2$ decreased the air-fuel equivalence ratio and the Brake Specific Diesel Fuel Consumption Efficiency by around 14–29 % and 4–31 %. In contrast, adding $H_2$ increased the Brake Fuel Conversion Efficiency by around 3–36 %. In addition, the Brake Thermal Efficiency increased in the presence of $H_2$ in the range of 3–37 % for the lower engine speed and 27–43 % for the higher engine speed compared with neat diesel. The dual-fuel mode resulted in lower CO and $CO_2$ emissions for the same power output. The emissions of hydrocarbons decreased with $H_2$ addition, except for the lower engine speed and the higher torque. However, the dual-fuel operation resulted in higher $NO_x$ emissions than neat diesel, with 2–6 % and 19–48 % increments for the lower and higher engine speeds. $H_2$ emerges as a versatile energy carrier with the potential to tackle current energy and emissions challenges; however, the dual-fuel strategy requires careful management of $NO_x$ emissions.

---

* Corresponding author.
  *E-mail address:* jorgeduarte@mail.uniatlantico.edu.co (J. Duarte-Forero).

## 1. Introduction

Although essential to the industry, energy, and transportation sectors, fossil fuels such as natural gas, oil, and coal contribute to a vast portion of the worldwide $CO_2$ emissions. The impacts of excessive $CO_2$ and other pollutants emissions are widely recognized: global warming [1], glaciers retreat [1], higher sea levels [2], and pollution-related public health problems [3]. Therefore, international treaties promote policies and mitigation strategies to reduce greenhouse emissions. For instance, the standard ISO 50001 sets the basis for incorporating low carbon sources and renewable energy systems [4]. Thus, both researchers and practitioners focus on exploring alternative energy sources [5] and carriers with reduced pollutant emissions [6] while also promoting the decentralization of energy systems [7].

Fossil fuels account for around 80 % of the current energy demand [8], which shows the imminent necessity for adjusting the conventional structure of energy production and consumption [9].

Hydrogen (H2) is a flammable, colorless, and odorless gaseous energy carrier in its molecular form. Therefore, $H_2$ represents a potential solution to energy storage and surplus energy utilization [10]. The absence of carbon atoms in $H_2$ results in CO- and $CO_2$-free combustion within a wide range of flammability limits [11]. In addition, $H_2$ features a high energy content per unit mass, the energy content of 1.0 kg of $H_2$ being equivalent to that of 2.6 kg of gasoline [12, 13]. Currently, $H_2$ production is still dominated (>48 %) by natural gas reforming [14]. The so-called green $H_2$ originates, for example, from renewable energy-based water electrolysis [15]. Nowadays, more reliable cells and electrochemical mechanisms optimize the overall performance, such as low-temperature electrolysis [16]. This method circulates a direct current through two electrodes in a solution, resulting in the fragmentation of $H_2O$ into $H_2$ and $O_2$ [17].

The world has around 1.2 billion passenger vehicles and 380 million commercial vehicles, and these numbers continue to increase. Transport is carried out almost entirely (>99%), with internal combustion engines that most likely use liquid fuels derived from petroleum [18]. Internal combustion engines have a wide range of applications, and all their parameters must be assessed to reveal their influence on performance and greenhouse gas emissions [19, 20]. Different technologies aim to increase the efficiency of these engines *via* waste heat recovery from exhaust gases. For example, thermoelectric generators [21, 22] represent a mature technology to improve fuel utilization. Likewise, evaluating different biofuels is a promising avenue to reduce pollutants emission and fuel consumption rates [23].

Published studies explore the effects of adding $H_2$ to internal combustion diesel engines. Experimental research assessed the impacts of adding $H_2$ to the inlet stream of compression-ignition (CI) engines. Marked variations in engine efficiency resulted from changing $H_2$ flow. The vehicle drivability did not show significant differences; however, exhaust gas temperature increased with $H_2$ addition [24]. Test results on a four-cylinder direct-injection turbocharged diesel engine operating with diesel and $H_2$ showed that the highest reduction in $CO_2$ emissions was around 46 %. On the other hand, the addition of $H_2$ to the engine increased $NO_x$ emissions at high loads [25].

Kathri et al. [26] investigated the performance of a single-cylinder, four-stroke compression-ignition engine after adding $H_2$ and biogas to diesel. They reported a 71 % reduction in Brake-Specific Diesel Fuel Consumption (BSDFC) and a 12 % reduction in Brake-Specific Energy Consumption (BSEC). In addition, HC, CO, and $NO_x$ emissions decreased by 5.7 %, 88 %, and 83 %. Similarly, Rajak et al. [27] performed tests contrasting diesel with $H_2$-diesel in a diesel engine. Smoke and $CO_2$ emissions and fuel consumption decreased at all loads. Notably, $NO_x$ emissions increased at high loads depending on the diesel replacement. For example, with the addition of 15 % $H_2$ at high loads, the specific fuel consumption decreased by 18 %, while $NO_x$ emissions increased by 21 %.

On the other hand, a computational study explored the $H_2$-diesel dual-fuel operation of a four-stroke direct injection compression ignition engine. The results showed that advancing the injection timing decreases the CO, soot, and HC emissions and increases $NO_x$ emissions [28]. Furthermore, experiments in light-duty and heavy-duty diesel engines showed that the addition of $H_2$ increased $NO_x$ emissions in the former case. However, $NO_x$ emissions slightly decreased in the heavy-duty engine while CO and particulate emissions decreased in both engines [29]. Finally, a study assessed the influence of Hydrogen Energy Share (HES) in a diesel engine. The results show that the heat release increased by around 46% and the efficiency by about 17%. Additionally, Soot, CO, and $CO_2$ decreased, while HC and $NO_x$ increased [30]. Overall, the literature shows the performance and emissions of $H_2$-diesel dual-fuel engines, but for a specific operation condition (*i.e.* a fixed engine speed and torque) or a limited operating range. Therefore, the present research covers a broader range of engine speed and torque to gain further insights into engine performance and emissions. This work contributes to a picture of engine performance and emissions for relevant engine speed and torque combinations, thus closing the knowledge gap towards implementing $H_2$ as a robust energy carrier.

In what follows, section 2 describes the experimental setup, operational procedures, and measurements. Then, engine performance and emissions are dealt with in Section 3. Engine performance includes Brake Specific Diesel Fuel Consumption (BSDFC), Brake Fuel Conversion Efficiency (BFCE), Brake Thermal Efficiency (BTE), and Volumetric Efficiency (VE). The studied gas emissions are CO, $CO_2$, HC, $O_2$, $NO_x$, and $SO_2$. Finally, the last section concludes with the final remarks on this research contribution.

## 2. Materials and methods

In what follows, we describe the main sections of the experimental setup and fuel properties. The section also includes the experimental design and the analysis of measurement uncertainty.

### 2.1. Experimental setup

The main sections of the setup are the engine-generator set, $H_2$ generator, fuel supply, load bank, and exhaust gas analyzers, as shown in Figure 1.

#### 2.1.1. Engine-generator set

The set consists of a single-cylinder, four-stroke, air-cooled compression ignition engine (model SK-MDF300, Sokan®) coupled to a generator (model SK-GD4000CL, Sokan®). Table 1 lists the specifications of the engine-generator set.

The data acquisition system includes sensors that provide real-time measurements of the variables listed in Table 2.

#### 2.1.2. $H_2$ generator

An in-house designed and built monopolar alkaline cell generates $H_2$ starting from a solution of distilled water and potassium hydroxide. Figure 2 depicts an assembled view of the alkaline cell and a closer view of the cathodic chamber. Table 3 summarizes the specifications of the monopolar alkaline cell designed and built in this study.

The electrolyzer incorporates two electrolyte storage tanks connected to the $H_2$ generation cell, as shown in Figure 3. The power source for the electrolyzer is alternating current at 110 V and 60 Hz. The $H_2$ and $O_2$ evolving from the electrodes pass through the electrolyte before passing through bubblers and reaching the storage tanks. $H_2$ and $O_2$ are temporarily stored in their respective tanks until they reach sufficient pressure to overcome the resistance imposed by the bubblers. The bubblers clean the gases by trapping water drops and vapor and enable a one-way flow by acting as a check valve. We installed two serial arresters for each gas storage for safety purposes, thus avoiding uncontrolled explosions of the stored gas due to flashbacks during the burning or injection of the fuel gas. The hydrogen injected into the engine is regulated using a flow meter.
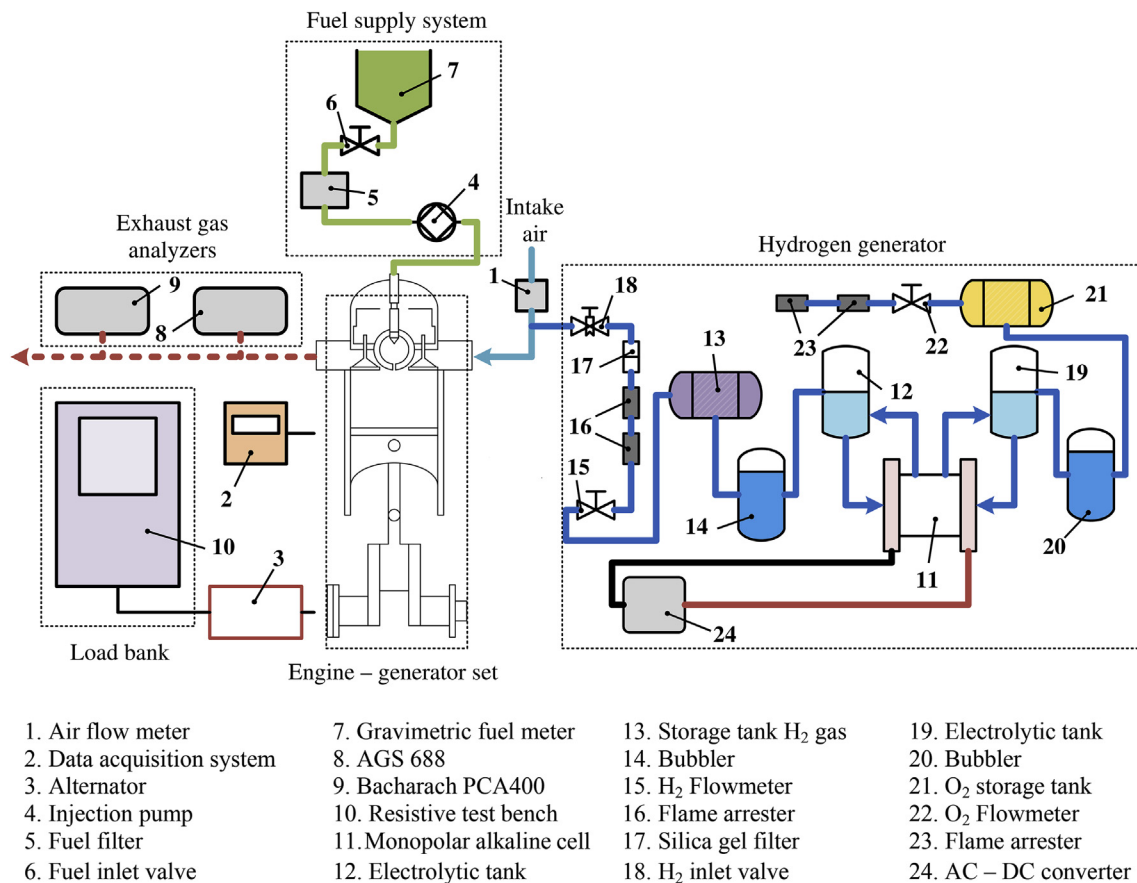
**Figure 1.** Experimental setup for the hydrogen-diesel dual operation experiments.

1. Air flow meter
2. Data acquisition system
3. Alternator
4. Injection pump
5. Fuel filter
6. Fuel inlet valve
7. Gravimetric fuel meter
8. AGS 688
9. Bacharach PCA400
10. Resistive test bench
11. Monopolar alkaline cell
12. Electrolytic tank
13. Storage tank $H_2$ gas
14. Bubbler
15. $H_2$ Flowmeter
16. Flame arrester
17. Silica gel filter
18. $H_2$ inlet valve
19. Electrolytic tank
20. Bubbler
21. $O_2$ storage tank
22. $O_2$ Flowmeter
23. Flame arrester
24. AC – DC converter

**Table 1.** Technical specifications of the engine-generator set.

| Engine, model SK-MDF300 Sokan® | |
|---|---|
| Rated Power | 3.5 kW @ 3600 rpm |
| Maximum power | 4.92 kW @ 3600 rpm |
| Cylinder bore | 78 mm |
| Cylinder stroke | 62.57 mm |
| Displacement | 296 cm$^3$ |
| Compression ratio | 20:1 |
| Intake system | Naturally aspirated |
| Injection system | Direct |
| Injection angle | 20° BTDC[a] |
| Generator, model SK-GD4000CL Sokan® | |
| Voltage | 120/240 VAC |
| DC output | 12 V |
| Maximum power | 3500 W |
| Nominal power | 3100 W |
| Nominal current | 26/13 A |

**Table 2.** Measured variables and sensors specifications of the data acquisition system.

| Variable | Sensor type | Accuracy | Measuring Range | Resolution |
|---|---|---|---|---|
| Temperature | Type K thermocouple | ±0.7% | -40 °C to 1100 °C | 0.1 °C |
| Pressure | Piezoresistive | ±0.3% | -100 kPa to 100 kPa | 0.001 kPa |
| Fuel mass flow rate | Gravimetric meter | ±2% | 0–16 g s$^{-1}$ | 0.0001 g s$^{-1}$ |
| Air mass flow rate | Hot wire | ±1.2% | 0–125 g s$^{-1}$ | 0.001 g s$^{-1}$ |
| Engine speed | Hall effect | ±0.03% | 5–9999 rpm | 1 rpm |
| Relative humidity | Capacitive | ±2% | 0–100% | 0.1 % |
| Atmospheric pressure | Digital barometer | ±2% | 30 kPa to 110 kPa | 0.3 kPa |
| Electric current | Hall effect | ±3% | 0–100 A | 0.01 A |

### 2.1.3. Fuel supply system and load bank

A needle valve regulates the flow of diesel fuel from a 10 L storage tank to the engine. The admission system allows controlling injection timing and duration. Diesel and $H_2$ flow separately through the intake manifold, thus avoiding backfire. The load bank incorporates power blocks of 335 W and 660 W, has an upper power limit of 3.5 kW and enables engine speed control.

### 2.1.4. Exhaust gas analyzer

A centrifugal fan extracts the exhaust gases through a 20 cm diameter circular duct. Table 4 summarizes the measurements carried out with two exhaust gas analyzers (model PCA 400, Bacharach®, and model AGS-688, Brain Bee®).

### 2.2. Fuel properties

Table 5 lists the properties of the fuels used in this study.

**Figure 2.** Assembled view of the monopolar alkaline cell.
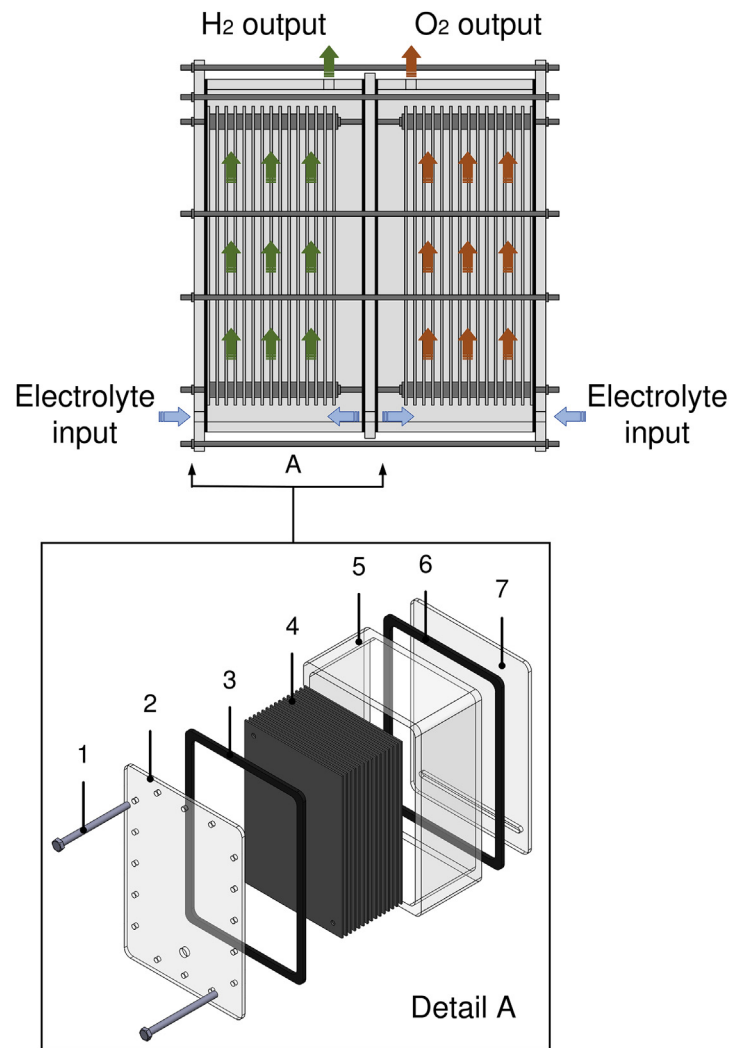
1. Clamping element    3. Packing    5. Body    7. Spacer
2. Clamping element    4. Electrode    6. Packing

**Table 3.** Technical specifications of the monopolar alkaline cell.

| Specification | Value/type |
|---|---|
| Electrolyte | KOH solution 20 % vol |
| Electrolyte capacity | 10 L |
| Hydrogen flow | 20 L min$^{-1}$ |
| Solution temperature | 40–50 °C |
| Body Material | PMMA |
| Electrode material | Stainless steel, 0.8 mm |
| Electrode orientation | Vertical |
| Active electrode area | 3200 mm$^2$ |
| Electrode spacing | 3 mm |
| Number of electrodes in the cathodic chamber | 18 |
| Number of electrodes in the anodic chamber | 18 |
| Supply voltage | 13.45 v |
| Cell voltage | 13.45 v |
| Cell current | 15.1 A |

### 2.3. Experimental design

The input variables were engine speed, torque, and hydrogen volumetric flow rate. The engine performance parameters include Brake Specific Diesel Fuel Consumption (BSDFC), Brake Fuel Conversion Efficiency (BFCE), Brake Thermal Efficiency (BTE), and Volumetric Efficiency. On the other hand, emissions include $O_2$ and $CO_2$, CO, NO, $NO_x$, $SO_2$, and HC. Figure 4 illustrates the input variables' levels and the engine characteristic curve. The experiments with $H_2$ used a volumetric flow rate of 20 L min$^{-1}$.

The study consists of 24 experimental runs, with three runs at each experimental condition. Statgraphics Centurion XVI.I software (Statgraphics Technologies, Inc) allowed randomizing the experiments to minimize unwanted effects caused by uncontrolled ambient factors. A typical experiment started by setting the engine parameters and initializing the analyzer software. The following steps consisted of opening valves and setting the flowmeter parameters. Then, we selected an operation mode, either neat diesel or $H_2$-diesel dual fuel. The acquired data included engine performance parameters and emissions. At the
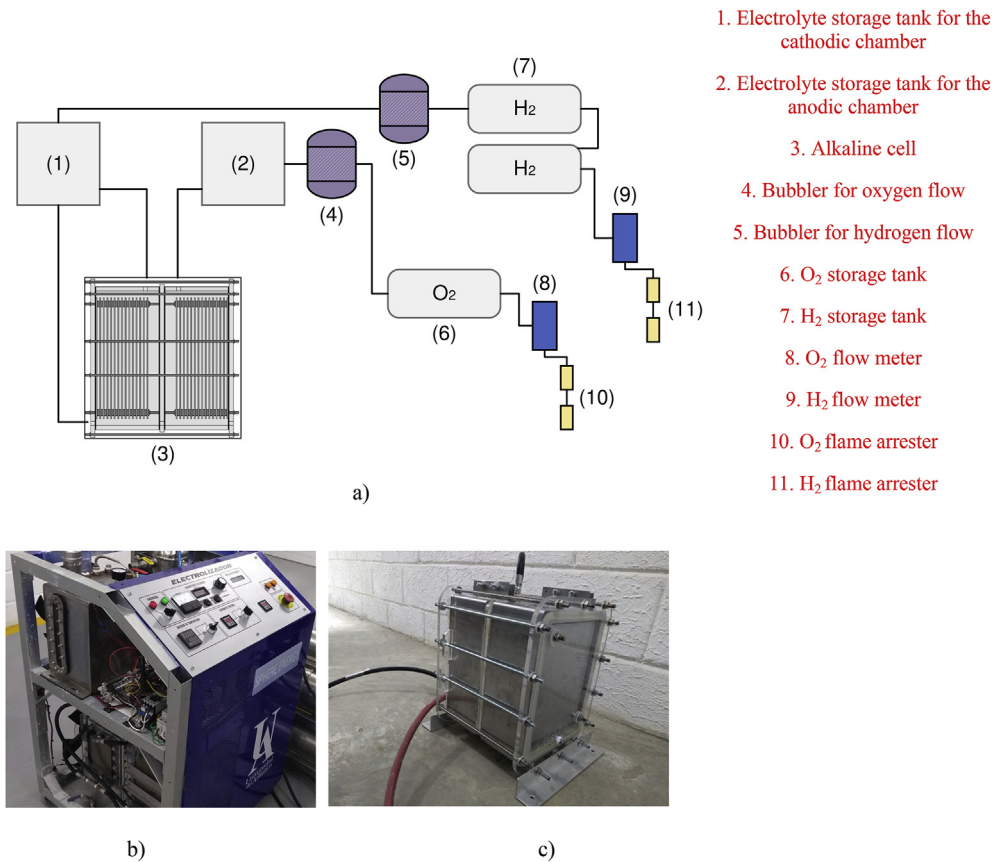
Figure 3. a) Schematic diagram of the electrolyzer; b) as-installed picture of the electrolyzer; c) monopolar alkaline cell.

**Table 4.** Technical specifications of the exhaust gas analyzers.

| Analyzer | Emissions | Range | Resolution |
|---|---|---|---|
| Bacharach PCA400 | $O_2$ | 0–20.9% | 0.10% |
| | CO | 0-40000 ppmv | 10 ppm |
| | $CO_2$ | 0–19.9% vol | 0.1 |
| | NO | 0-3000 ppmv | 1 ppmv |
| | $NO_x$ | 0-500 ppmv | 1 ppmv |
| | $SO_2$ | 0-5000 ppmv | 1 ppmv |
| AGS-688 | HC | 0-9999 ppmv | 1 ppmv |

**Table 5.** Properties of the mineral diesel and hydrogen.

| Properties | Diesel | $H_2$ |
|---|---|---|
| Lower Heating Value (LHV), MJ kg$^{-1}$ | 42.5 | 119.7 |
| Density at NTP[a], kg m$^{-3}$ | 860 | 0.0899 |
| Flammability limits in air, vol % | 0.7–5 | 4.0–75.0 |
| Auto-ignition temperature in air, °C | 553 | 858 |
| Stoichiometric air-to-fuel ratio (A/F) | 14.7 | 34.3 |
| Normal boiling point, °C | ~150–380 | -252.9 |
| Sulfur content, mg kg$^{-1}$ (ppmw) | <50 | - |

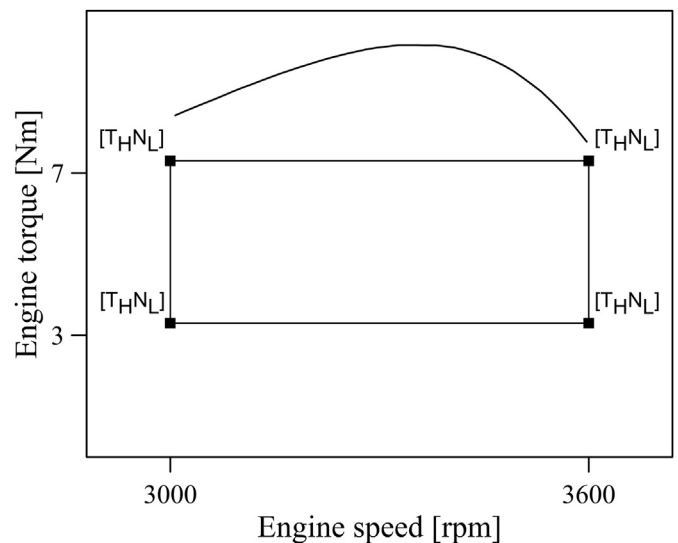[a] Normal Temperature and Pressure, 101.325 kPa and 293.15 K.



Figure 4. Experimental levels of the input variables engine speed and torque for the experimental design. Subscripts H and L refer to the input variable levels, T represents torque, and N represents engine speed. The upper curve corresponds to the engine characteristic curve.

beginning of the campaign, we measured output power as a function of engine speed and torque for the operation with neat diesel and $H_2$-diesel dual fuel. The relative error based on the standard deviation (over three experiments) was within 2%, indicating excellent repeatability at each experimental condition.

### 2.4. Uncertainty analysis

Physical measurements in experimental tests are exposed to different sources of error, such as environmental conditions, calibration, and type of instrument, among others. Due to the above, it is necessary to carry out an uncertainty analysis to guarantee the reliability of the results obtained

experimentally. Type A evaluation method was used to calculate uncertainty based on a statistical analysis of a set of measurements. The best estimate ($\overline{y}$) of a series of measurements ($y_1$, $y_2, y_3 \ldots y_n$) was calculated from Eq. (1).

$$\overline{y} = \frac{\sum_{i=1}^{n} y_i}{n} \tag{1}$$

where $n$ represents the number of records of each measured variable. The standard deviation ($\sigma$) of the set of measurements was calculated *via* Eq. (2).

$$\sigma = \sqrt{\frac{\sum_{i=1}^{n} (y_i - \overline{x})^2}{n-1}} \tag{2}$$

The uncertainty calculation ($u$) used the standard deviation, as indicated in Eq. (3).

$$u(y) = \frac{\sigma}{\sqrt{n}} \tag{3}$$

In the case of variables that present different sources of uncertainty, a combined uncertainty ($u_c$) was calculated, as shown in Eq. (4).

$$u_c = \sqrt{u_{(x_1)}^2 + u_{(x_2)}^2 + u_{(x_3)}^2 + \ldots + u_{(x_n)}^2} \tag{4}$$

Table 6 shows the uncertainty of the parameters measured in the experimental tests.

The uncertainty associated with the instrumentation (Type B) is 10% of the expanded uncertainty. Therefore Type A is the most representative measurement uncertainty.

## 3. Results and discussion

This section presents and discusses the experimental results, starting with the engine performance parameters and then covering engine emissions.

### 3.1. Engine performance parameters

Eq. (5) gives the air-fuel ratio (*AF*). On the other hand, the air-fuel equivalence ratio ($\phi$), given by Eq. (6), indicates whether the mixture is lean ($\phi < 1$), rich ($\phi > 1$), or stoichiometric ($\phi = 1$). The symbol $m$ represents mass, subscripts $a$ and $f$ refers to air and fuel, and subscript $s$ indicates the stoichiometric condition.

$$AF_s = \left(\frac{m_a}{m_f}\right)_s \tag{5}$$

$$\phi = \frac{AF_s}{AF} \tag{6}$$

**Table 6.** Uncertainty associated with measurement instruments.

| Parameter | Uncertainty [%] |
|---|---|
| Temperature | ±0.5 |
| Pressure | ±1.3 |
| Fuel mass flow rate | ±1.2 |
| Air mass flow rate | ±1.0 |
| Engine speed | ±0.1 |
| $O_2$ | ±1.3 |
| CO | ±0.9 |
| $CO_2$ | ±2.0 |
| $NO_x$ | ±0.7 |
| $SO_2$ | ±0.6 |
| HC | ±1.5 |

Figure 5 shows that adding $H_2$ leads to lower $\phi$ for all the evaluated engine speed and torque levels. Note that $AF_s$ for diesel amounts to 14.7, which is less than half the corresponding value for $H_2$. Therefore, even relatively low hydrogen amounts could significantly influence $\phi$. This result is consistent with a moderate increase in the air mass flow rate ($\dot{m}_a$) and a decrease in the diesel mass flow rate ($\dot{m}_d$), leading to higher AF in all cases.

#### 3.1.1. Hydrogen energy share (HES)

Eq. (7) gives *HES*, which provides the energy contribution of $H_2$ in the dual-fuel operation. In Eq. (3), *LHV* indicates the Low Heating Value of the fuel.

$$HES = \frac{\dot{m}_{H2} \cdot LHV_{H2}}{\dot{m}_{H2} \cdot LHV_{H2} + \dot{m}_d \cdot LHV_d} \cdot 100\% \tag{7}$$

In this work, *HES* varied in the range of 18–37%, with the highest *HES* value corresponding to the lower levels of engine speed and torque. Increasing engine speed at constant torque decreased *HES*, and a similar trend resulted from increasing torque at constant engine speed.

#### 3.1.2. Brake Specific Diesel Fuel Consumption (BSDFC) and Brake Fuel Conversion Efficiency (BFCE)

Eq. (8) gives *BSDFC*, the ratio of the diesel mass flow rate ($\dot{m}_d$) and the engine Brake Power (*BP*).

$$BSDFC = \frac{\dot{m}_d}{BP} \tag{8}$$

Figure 6a reveals a consistent decrease in *BSDFC* when comparing the dual-fuel with the neat diesel operation. *BSDFC* dropped by around 27 % and 4 % for the lower engine speed and the higher and lower torque levels, respectively. The corresponding results for the higher engine speed were 21 and 31 %.

Eq. (9) gives *BFCE*, which relates *BP* to the fuel chemical energy.

$$BFCE = \frac{BP}{\dot{m}_d \cdot LHV_d + \dot{m}_{H2} \cdot LHV_{H2}} \cdot 100\% \tag{9}$$

Figure 6b reveals that the dual-fuel operation increased BFCE compared to the neat diesel operation. Some effects that could contribute to this outcome are the additional water vapor from $H_2$ combustion, the
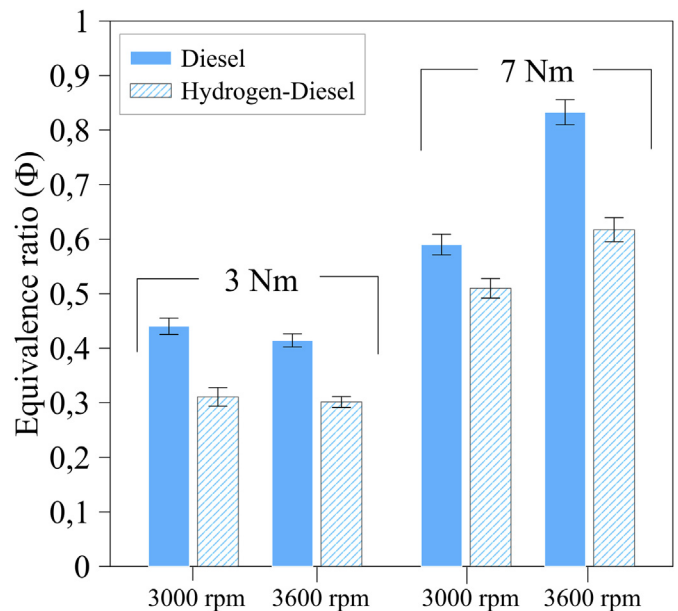


**Figure 5.** Influence of fuel type on the equivalence ratio for different levels of engine speed and torque.
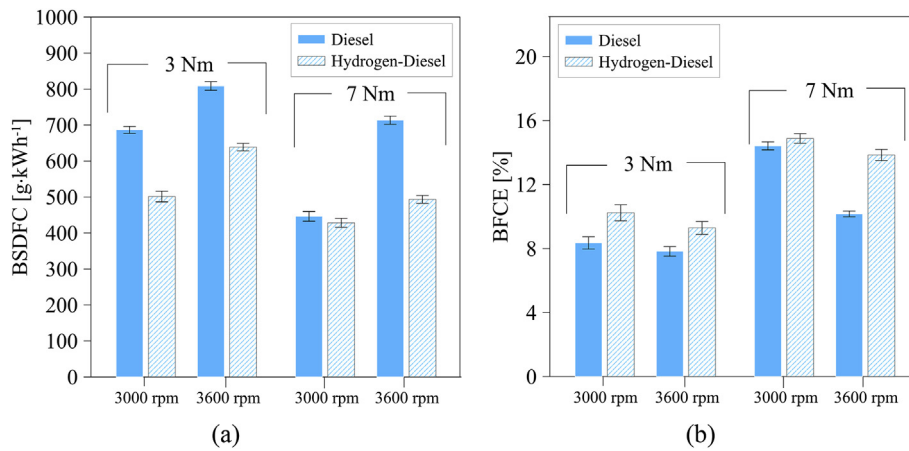
**Figure 6.** (a) Brake Specific Diesel Fuel Consumption (*BSDFC*), and (b) Brake Fuel Conversion Efficiency (*BFCE*) for different levels of engine speed and torque.

duration of diesel fuel injection, and fluctuations in diesel ignition delay [31, 32].

*3.1.3. Brake Thermal Efficiency (BTE) and volumetric efficiency (VE)*

Eq. (10) gives *BTE*, which relates *BP* to the fuel chemical energy of the operation with neat diesel.

$$BTE = \frac{BP}{\dot{m}_{d,100\%} \cdot LHV_d} \cdot 100\% \qquad (10)$$

Figure 7a reveals a consistent increase in *BTE* when comparing the dual-fuel operation with only diesel. This result indicates enhanced mixing, lower losses, faster combustion, and reduced pumping work for diesel [33]. *BTE* increased by around 37 and 4 % for the lower engine speed and the higher and lower torque levels, respectively. The corresponding increments for the higher engine speed were 27 and 43 %.

Eq. (11) gives the Volumetric Efficiency (*VE*), the ratio between the actual and the maximum air mass flow rate flowing through the engine. In Eq. (6), $\rho$ represents density, *V* volume, *N* engine speed, and *DV* displaced volume. Additionally, $n_r$ represents the number of crankshaft rotations for a complete engine cycle, which equals two for a 4-stroke engine.

$$VE = \frac{\dot{m}_a \cdot n_r}{\rho_a \cdot DV \cdot N} \cdot 100\% \qquad (11)$$

Figure 7b shows that, compared with the neat diesel operation, *VE* increased for all the load conditions except for the higher engine speed and torque. *VE* increased by approximately 3.5–11 % in the first three

operation modes because the throttle is fully open. However, at an engine speed of 3600 rpm and a 7 Nm torque, $H_2$ displaces air, which decreases *VE* by around 6.7 % [34].

The addition of $H_2$ resulted in a higher air-fuel equivalence ratio ($\phi$) for both torque levels at an engine speed of 3000 rpm. On the other hand, there was a reduction in $\phi$ for both torque levels at 3600 rpm. HES presented a variation between 18-37 %, evidencing the highest value of HES at 3000 rpm and a torque of 3 Nm. HES decreased with increasing engine speed at constant torque, as it did when the torque increased at constant engine speed. BSDFC decreased by about 27 and 4 % for the lowest engine speed at the highest and lowest torque levels. In addition, corresponding results were obtained for the highest engine speed of 21% and 31%.

BTE increased by about 37 and 4 % for the lowest engine speed at the highest and lowest torque levels. The corresponding results for the highest engine speed were 27% and 43%, and the VE increased for all load conditions; this was approximately between 3.5 and 11% in the first three operating modes. However, at a higher engine speed equal to 3600 rpm and torque of 7 Nm, VE decreases by about 6.7 %.

## 3.2. Emissions

The emissions measured in our experiments were CO, $O_2$, $CO_2$, HC, $NO_x$, and $SO_2$. In what follows, we discuss each of them in the same order.

### 3.2.1. CO emission

Figure 8a shows a slight decrease in CO emission (from 0.06 to 0.04 v/v %) for the neat diesel operation when increasing torque from 3 to 7 Nm at the lower engine speed. The corresponding results at the higher engine
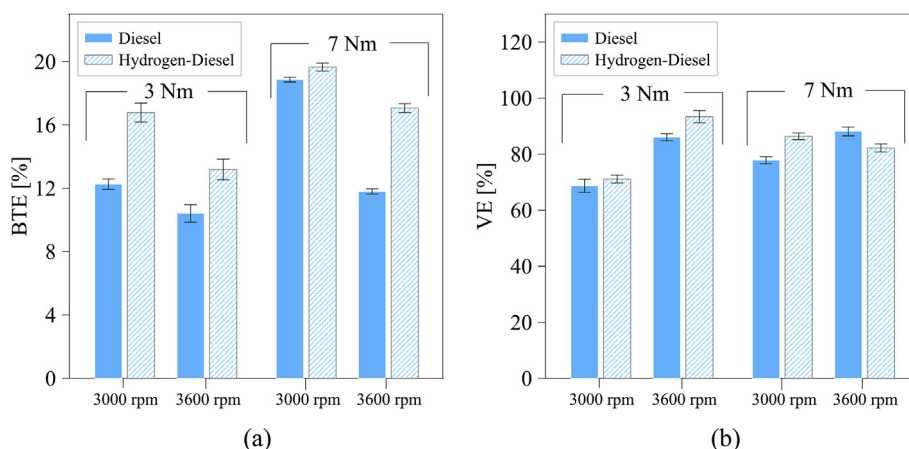


**Figure 7.** (a) Brake Thermal Efficiency (*BTE*), and (b) Volumetric Efficiency (*VE*) for different levels of engine speed and torque.

speed feature the opposite trend in CO emission with a 10-fold increase. Likewise, increasing engine speed at the lower torque resulted in similar CO emission, but there was a striking 16-fold increase in CO emission at the higher torque. The increments in CO emission are consistent with increments in $\phi$ because of the richer mixture, which agrees with a published emission map for CO as a function of engine speed and torque [35]. Figure 8a also shows similar CO emission for the dual-fuel operation when increasing torque from 3 to 7 Nm at the lower engine speed and the lower engine speed and higher torque. There was also a notable 6-fold increase in CO emission at the higher engine speed and torque. Finally, compared with the only-diesel mode, the dual-fuel mode always resulted in lower CO

emission, especially at the higher engine speed and torque, with corresponding results of 0.65 and 0.19 v/v %.

Previous experimental studies on $H_2$-diesel dual-fuel operation disclose findings consistent with our results. Pavlos et al. revealed a reduction of 94% with a 98% of hydrogen energy ratio, around 34%–95% and 16%–65% in three different studies, respectively [36, 37, 38]. Koten et al. showed a maximum decrease of 12.09% in a four-stroke diesel with a direct injection engine [39]. CO emissions dropped by around 25–71 % in the dual-fuel mode, and the effect was most evident at the higher engine speed and torque. The equivalence ratio decreased with $H_2$ addition, reducing CO emissions [40]. Relatively high
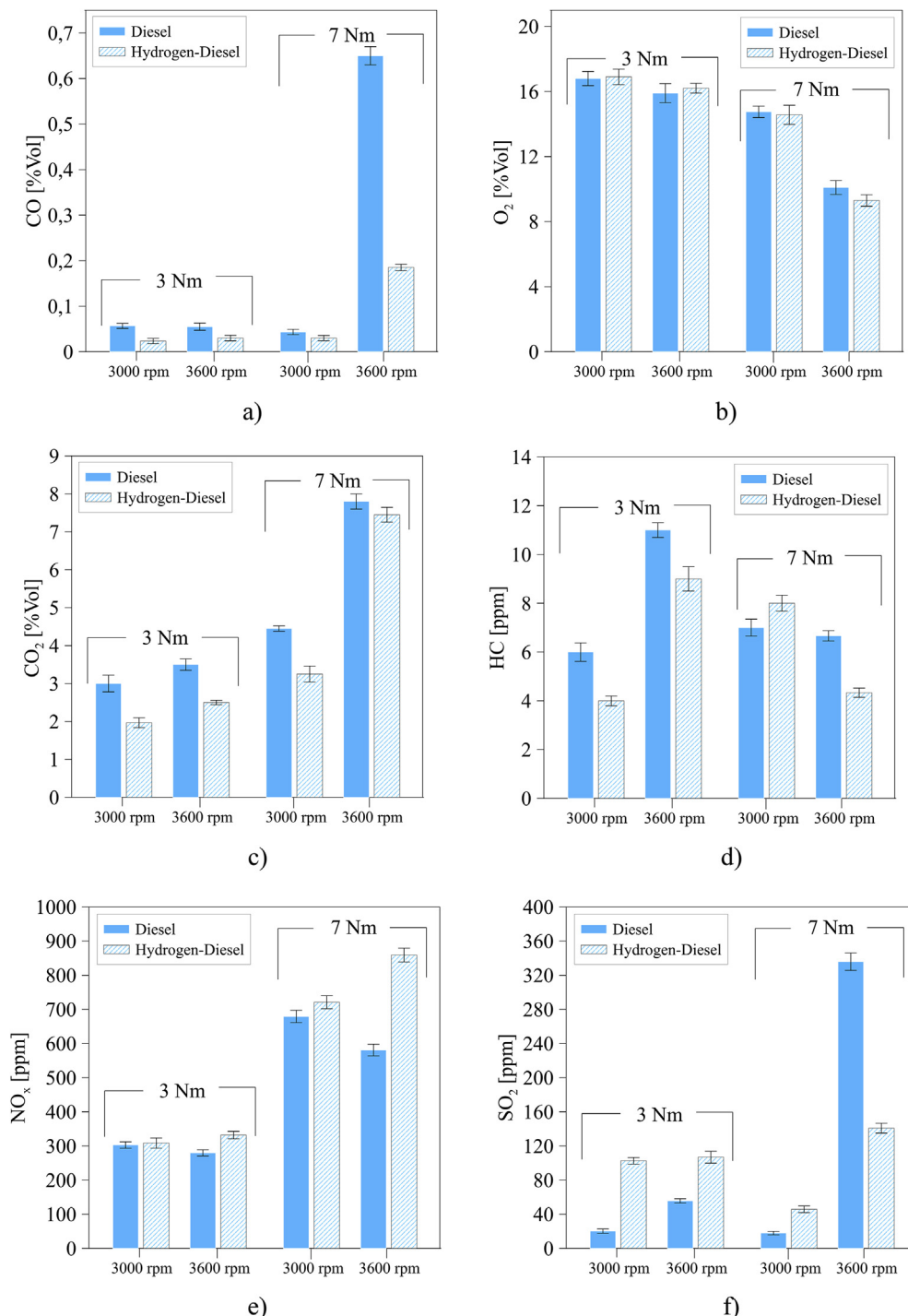


Figure 8. Pollutant emissions for neat diesel and $H_2$-diesel dual fuel: a) CO; b) $O_2$; c) $CO_2$; d) HC; e) $NO_x$; f) $SO_2$.

in-cylinder temperature characterizes the dual-fuel mode, and this condition reduces CO emission by favoring its conversion into $CO_2$ [41].

### 3.2.2. $O_2$ emission

The dependence of $O_2$ emission on both engine speed and torque shows an inverse relation for the operation with neat diesel [35]. Our results for $O_2$ emission agree with those findings, as shown in Figure 8b. For neat diesel, increasing torque from 3 to 7 Nm at an engine speed of 3000 rpm decreases $O_2$ emission by around 12%. A similar increase in torque at 3600 rpm also reduces $O_2$ emission by about 36 %. Conversely, increasing engine speed from 3000 rpm to 3600 rpm for the lower and higher torque resulted in respective drops in $O_2$ emission of about 5 and 32 %. The dual-fuel operation only shows minor differences in $O_2$ emission (<2%) compared with the operation with neat diesel, consistent with the moderate HES in our study. Studies reporting $O_2$ emissions for dual fuel operation are scarce, although assessing $O_2$ emissions provides valuable insight into combustion quality.

### 3.2.3. $CO_2$ emission

The results show a direct proportion for the dependence of the $CO_2$ emission on both engine speed and torque when operating with neat diesel [35]. Figure 8c indicates that increasing torque from 3 to 7 Nm at 3000 rpm raised $CO_2$ emission by around 48% when operating with pure diesel. For the same fuel and torque change, but at 3600 rpm, $CO_2$ emission increased by approximately 122 %. Additionally, increasing engine speed from 3000 rpm to 3600 rpm for the lower and higher torque resulted in respective increments in $CO_2$ emission of about 17% and 73%. For an engine speed of 3000 rpm and dual fuel operation, Figure 8c indicates that increasing torque from 3 to 7 Nm raised $CO_2$ emission by about 65%. Likewise, the same torque change at an engine speed of 3600 rpm increased $CO_2$ by around 2-fold. When engine speed was raised from 3000 rpm to 3600 rpm, $CO_2$ emission increased by approximately 25 % for the lower torque and 127 % for the higher torque. Lastly, the dual-fuel mode always resulted in lower CO emission than the neat diesel mode, although this difference decreased considerably at the higher engine speed and torque.

$H_2$ is a carbon-free molecule, so its addition to the intake air reduces the emission of $CO_2$ for given output power. Published studies on $H_2$-diesel dual-fuel engines also report similar results, where it could be noted maximum reductions of 45.7 %, 11.5 %, and 39.0 % with different engines and hydrogen contribution percentages [25, 39, 40]. A common rail direct injection diesel engine featured a $CO_2$ maximum reduction of 14% [42]. Other studies showed a maximum reduction of 17 % in a single-cylinder diesel engine with a higher capacity [43]. Our results show a drop in $CO_2$ emission of about 5–34 %, the lower result corresponding to the higher engine speed and torque.

### 3.2.4. HC emission

The incomplete combustion of hydrocarbons in the fuel causes HC emissions. Figure 8d reveals that increasing torque from 3 to 7 Nm at an engine speed of 3000 rpm raises HC emissions by around 33 % for neat diesel operation. A similar increment in torque at 3600 rpm shows the opposite trend in HC emissions, with a drop of about 41 %. Furthermore, increasing engine speed from 3000 to 3600 rpm at a torque of 3 Nm raised HC emissions by around 83 %. Again, the same increment in engine speed at the higher torque level decreased HC emissions by approximately 19 %. The dual-fuel operation features HC emissions trends like those described above for pure diesel. Additionally, increasing torque at the lower engine speed and increasing engine speed at the lower torque raised HC emissions by around 75 % and 125 %, respectively. Conversely, increasing torque at the higher engine speed and increasing engine speed at the higher torque diminished HC emissions by 50 and 36 %, respectively.

The addition of $H_2$ to the air intake port could result in fast combustion, high in-cylinder temperature, and lower carbon in the fuel per output power unit. The expected output is a reduction in HC emissions.

However, Figure 8d contradicts this expectation at the lower engine speed and higher torque.

Several studies report significant reductions in HC emissions for the dual-fuel operation compared with neat diesel [44, 45]. On the other hand, in their review, Rosha et al. [40] list some studies in which HC emissions increased under dual-fuel operation compared with neat diesel. Other researchers also report an increment in HC emissions for a specific load and HES (hydrogen energy sharing) level [43, 46]. These contrasting results suggest that, at certain operation conditions, the addition of $H_2$ could result in reduced combustion efficiency.

### 3.2.5. $NO_x$ emission

$NO_x$, composed of NO and $NO_2$, is one of the main challenges for internal combustion engines, especially under dual-fuel operation. According to Figure 8e, $NO_x$ emissions for neat diesel increased by around 124 % when torque increased from 3 Nm to 7 Nm at an engine speed of 3000 rpm. Under an engine speed of 3600 rpm, the same increase in torque raised $NO_x$ emissions by around 108 %. For the lower and higher torque levels, increasing engine speed from 3000 rpm to 3600 rpm raised $NO_x$ emissions by about 7 and 14 %, respectively. On the other hand, for a dual-fuel operation, results indicate that increasing torque from 3 to 7 Nm boosts $NO_x$ emissions by around 133 and 159 % at respective engine speeds of 3000 rpm and 3600 rpm. Likewise, increasing engine speed from 3000 rpm to 3600 rpm under dual-fuel operation raised $NO_x$ emissions by 7 and 19 % for the lower and higher torque levels, respectively. A direct proportion characterizes $NO_x$ emissions dependence on torque, while $NO_x$ emissions are almost independent of engine speed for the operation with neat diesel [35]. The general behavior demonstrated that rising the engine power causes an increase in the combustion chamber temperature, thus exacerbating $NO_x$ emissions. $H_2$ has a relatively high heating value, which induces higher combustion temperatures, as highlighted by Jamrozik et al. [47].

### 3.2.6. $SO_2$ emission

For neat diesel and an engine speed of 3000 rpm, Figure 8f indicates that increasing torque from 3 to 7 Nm decreased $SO_2$ emission by about 11 %. Contrarily, the same torque change at an engine speed of 3600 rpm increased $SO_2$ emission by around 508 %. When engine speed was raised from 3000 rpm to 3600 rpm, $SO_2$ emission increased by approximately 168 % for the lower torque and 1724 % for the higher torque. On the other hand, increasing torque from 3 to 7 Nm at an engine speed of 3000 rpm decreased $SO_2$ emission by 56 % for dual-fuel operation. A similar increment in torque at 3600 rpm shows the opposite trend in $SO_2$ emission, which increased by around 31 %.

Furthermore, increasing engine speed from 3000 to 3600 rpm at a torque of 3 Nm raised $SO_2$ emission by around 4.2 %. Contrarily, the same increment in engine speed at the higher torque level increased $SO_2$ emissions by about 210 %. Comparing the neat diesel and dual-fuel operations shows that starting from 3000 rpm, adding $H_2$ increased $SO_2$ emission at the exhaust for both torque values. Furthermore, adding $H_2$ also increased $SO_2$ emission for the operation at 3600 rpm and 3 Nm. Lastly, $SO_2$ emissions decreased significantly under dual-fuel operation in the most demanding condition.

$SO_2$ depends on fuel sulfur content, excess air, and burned fuel [48]. Therefore, adding $H_2$ favors the formation of $SO_2$ in the first three modes of operation because the throttle was always opened, and the air consumption was higher in the dual-fuel mode. In contrast, there was a decrease in $SO_2$ emissions in the most demanding mode of operation since the air consumption decreased compared with neat diesel. In addition, the decrease in air consumption favors the decrease in $SO_2$ emissions because $H_2$ displaces the oxygen in the air, which leads to a lower formation of $SO_2$, which is consistent with published results [47, 49].

A first indication of the economic viability of the technical proposal presented in this research results from analyzing the influence of adding

$H_2$ on engine economy. The cost rate of output power ($\dot{C}_w$, USD kWh$^{-1}$) was determined *via* Eq. (12).

$$\dot{C}_w = \frac{108600\rho_f \cdot \dot{m}_f}{\pi T \cdot \omega} \tag{12}$$

where $\rho_f$ (USD kg$^{-1}$) is the price of diesel fuel, $\dot{m}_f$ (kg s$^{-1}$) the mass flow of diesel fuel, T (kNm) the torque, and $\omega$ (rev min$^{-1}$) the rotational speed. To determine $\rho_f$, a diesel fuel price of 1.11 USD per liter was considered [47], with a density of 860 kg m$^{-3}$ (see Table 5), which resulted in 1.29 USD kg$^{-1}$.

Adding $H_2$ could reduce the cost of the generated power, depending on the cost of both $H_2$ and diesel. For a low load condition (a torque of 3 Nm), $H_2$ could enable a 23% reduction in the economic cost of power output. In the case of high load conditions (7 Nm), a cost reduction of 16% could be reached. On average, under the engine test conditions, a $\dot{C}_w$ of 0.87 USD kWh$^{-1}$ and 0.69 USD kWh$^{-1}$ were obtained for diesel and hydrogen-diesel mixture, respectively. This result implies that if the cost of $H_2$ generation is less than 0.18 USD kWh$^{-1}$, a net economic benefit would be achieved with the partial replacement of diesel with $H_2$. The $H_2$ generation cost will be determined by the renewable electricity source and the electrolyzer technology (PEM or alkaline) [51]. In addition, there will be other benefits related to the dual $H_2$-diesel operation, specifically the reduction of polluting emissions and the potential access to economic benefits due to support policies [47].

## 4. Conclusions and future outlook

This work presents an experimental assessment of performance and emissions for a single-cylinder, four-stroke, air-cooled compression ignition engine with neat diesel and $H_2$-diesel as fuels. Previous studies typically show the performance and emissions of $H_2$-diesel dual-fuel engines for a specific operation condition (*i.e.* a fixed engine speed and torque) or a limited operating range. In contrast, our experiments covered engine speed levels of 3000 and 3600 rpm, and torque levels of 3 and 7 Nm. In addition, an in-house designed alkaline cell generated the $H_2$ for partial diesel substitution.

Adding $H_2$ decreased the air-fuel equivalence ratio because $H_2$ displaced air in the engine. The extent of the decrease in Brake Specific Diesel Fuel Consumption under dual-fuel operation depended on engine speed and torque, and the best result corresponded to the most demanding operation mode. The dual-fuel operation mode also decreased the Brake Fuel Conversion Efficiency, consistent with the effect of water vapor from $H_2$ combustion. On the other hand, the Volumetric Efficiency, *i.e.*, the ratio between the actual and the maximum air mass flow rate, increased with $H_2$ addition for all the load conditions except at the highest power output.

The $H_2$-diesel dual-fuel mode resulted in markedly lower CO and $CO_2$ emissions than the operation with neat diesel for the same output power. The emissions of hydrocarbons decreased with $H_2$ addition, except for the lower engine speed and the higher torque. This result indicates that, at certain operation conditions, adding $H_2$ could result in reduced combustion efficiency. The dual-fuel operation showed minor changes in $O_2$ emissions than neat diesel, consistent with the relatively low Hydrogen Energy Sharing. The hydrogen-diesel dual-fuel mode resulted in higher $NO_x$ emissions than the operation with neat diesel, while the difference in $SO_2$ emissions depended on the engine speed and torque levels.

Although fossil fuels are still the predominant energy source for internal combustion engines, $H_2$ enrichment represents a robust alternative to tackle greenhouse emissions. The integration of green-$H_2$ production systems, namely electrolyzes, demonstrated versatility to operate simultaneously in internal combustion engines, reinforcing its implementation. The dual-fuel strategy can increase combustion stability and thermal efficiency while decreasing fuel consumption and $CO_2$, CO, and unburned hydrocarbons emissions. $H_2$ emerges as a versatile energy carrier with the potential to tackle current energy and emissions

challenges, and the $H_2$-diesel dual strategy is a suitable alternative for compression ignition engines. However, the results show that relatively high $NO_x$ emissions are a significant drawback. Besides, there is still room for enhancing power output within a wide range of engine speeds and torque using direct injection. The engine's durability and reliability are vital concerns to be tackled *via* dedicated tests.

The present study is limited to the analysis of the effects of $H_2$ in compression-ignition internal combustion engines, used mainly for power generation. Additionally, the investigation used a fixed hydrogen mass flow rate and did not measure soot emission. Future efforts should investigate the sustainability features of the results obtained using sustainability assessment tools such as life cycle assessment, energy and exergy analyses, and their combination [50]. Other research needs are further clarifying the effect of exhaust gas recirculation in the entire load range [51], diesel injection strategies to accomplish stable combustion [51], oxygenate additives [52], and knocking at high $H_2$ energy share [53].

## References

[1] A. Kumar, J. Yadav, R. Mohan, Global warming leading to alarming recession of the Arctic sea-ice cover: insights from remote sensing observations and model reanalysis, Heliyon 6 (2020).

[2] M. Siegert, R.B. Alley, E. Rignot, J. Englander, R. Corell, Twenty-first century sea-level rise could exceed IPCC projections for strong-warming futures, One Earth 3 (2020) 691–703.

[3] H.K.S. Panahi, M. Dehhaghi, J.E. Kinder, T.C. Ezeji, A review on green liquid fuels for the transportation sector: a prospect of microbial solutions to climate change, Biofuel Res. J. 6 (2019) 995–1024.

[4] V. António, F. José, M. Santos, Energy management system ISO 50001 : 2011 and energy management for sustainable development, Energy Pol. 133 (2019) 110868.

[5] A. Coram, D.W. Katzner, Reducing fossil-fuel emissions: dynamic paths for alternative energy-producing technologies, Energy Econ. 70 (2018) 179–189.

[6] G. Amador, J.D. Forero, A. Rincon, A. Fontalvo, A. Bula, R.V. Padilla, W. Orozco, Characteristics of auto-ignition in internal combustion engines operated with gaseous fuels of variable methane number, J. Energy Resour. Technol. 139 (4) (2017), 042205.

[7] Q. Wang, X. Yang, Investigating the sustainability of renewable energy – an empirical analysis of European Union countries using a hybrid of projection pursuit fuzzy clustering model and accelerated genetic algorithm based on real coding, J. Clean. Prod. 268 (2020) 121940.

[8] T. Ahmad, D. Zhang, A critical review of comparative global historical energy consumption and future demand: the story told so far, Energy Rep. 6 (2020) 1973–1991.

[9] S. Adams, E. Kwame, M. Klobodu, A. Apio, Renewable and nonrenewable energy, regime type and economic growth, Renew. Energy 125 (2018) 755–767.

[10] M. Khzouz, E.I. Gkanas, A. Girella, T. Statheros, C. Milanese, D. Chimica, C. Fisica, Sustainable hydrogen production via LiH hydrolysis for unmanned air vehicle (UAV) applications, Int. J. Hydrogen Energy 45 (2020) 5384–5394.

[11] C. Ghenai, M. Bettayeb, B. Brdjanin, A.K. Hamid, Hybrid solar PV/PEM fuel Cell/ Diesel Generator power system for cruise ship: a case study in Stockholm, Sweden, Case Stud. Therm. Eng. 14 (2019) 100497.

[12] B. Widera, Renewable hydrogen implementations for combined energy storage, transportation and stationary applications, Therm. Sci. Eng. Prog. 16 (2020) 100460.

[13] M. Koc, N. Tukenmez, M. Ozturk, Development and thermodynamic assessment of a novel solar and biomass energy based integrated plant for liquid hydrogen production, Int. J. Hydrogen Energy 45 (2020) 34587–34607.

[14] T. Sinigaglia, F. Lewiski, S. Eduardo, S. Martins, J. Cezar, M. Siluk, Production , storage, fuel stations of hydrogen and its utilization in automotive applications-a review, Int. J. Hydrogen Energy 42 (2017) 24597–24611.

[15] W. Martinez, E. Souza, A. Pedroni, J. Carvalhoa, V. Andrade, E. Sydneyb, Hydrogen: current advances and patented technologies of its renewable production, J. Clean. Prod. (2020) 124970.

[16] P. Olivier, C. Bourasseau, P.B. Bouamama, Low-temperature electrolysis system modelling: a review, Renew. Sustain. Energy Rev. 78 (2017) 280–300.

[17] I. Dincer, C. Acar, Innovation in hydrogen production, Int. J. Hydrogen Energy 42 (2017) 14843–14864.

[18] H. Ambarita, Performance and emission characteristics of a small diesel engine run in dual-fuel (diesel-biogas) mode, Case Stud. Therm. Eng. 10 (2017) 179–191.

[19] Y. Rathore, D. Ramchandani, R.K. Pandey, Experimental investigation of performance characteristics of compression-ignition engine with biodiesel blends of Jatropha oil & coconut oil at fixed compression ratio, Heliyon 5 (11) (2019), e02717.

[20] M. Vijayakumar, P.M. Kumar, Performance and emission characteristics of compression-ignition engine handling biodiesel blends with electronic fumigation, Heliyon 5 (4) (2019), e01480.

[21] R. Ramírez-Restrepo, A. Sagastume-Gutiérrez, J. Cabello-Eras, B. Hernández, J. Duarte-Forero, Experimental study of the potential for thermal energy recovery with thermoelectric devices in low displacement diesel engines, Heliyon 7 (11) (2021), e08273.

[22] R. Ramírez, A. Gutiérrez, J. Eras, K. Valencia, B. Hernández, J. Duarte, Evaluation of the energy recovery potential of thermoelectric generators in diesel engines, J. Clean. Prod. 241 (2019) 118412.

[23] G. Valencia, C. Acevedo, J. Duarte, Combustion and performance study of low-displacement compression ignition engines operating with diesel–biodiesel blends, Appl. Sci. 10 (3) (2020) 907.

[24] M. Shirk, T. Mcguire, G. Neal, D. Haworth, Investigation of a hydrogen-assisted combustion system for a light-duty diesel vehicle, Int. J. Hydrogen Energy 33 (2008) 7237–7244.

[25] N. Castro, M. Toledo, G. Amador, An experimental investigation of the performance and emissions of a hydrogen-diesel dual fuel compression ignition internal combustion engine, Appl. Therm. Eng. 156 (2019) 660–667.

[26] N. Khatri, K.K. Khatri, Hydrogen enrichment on diesel engine with biogas in dual fuel mode, Int. J. Hydrogen Energy 45 (2020) 7128–7140.

[27] U. Rajak, P. Nashine, T. Nath, A. Pugazhendhi, Performance and emissions analysis of a diesel engine using hydrogen enriched n-butanol, diethyl ester and Spirulina microalgae biodiesel, Fuel 271 (2020) 117645.

[28] G. Tripathi, P. Sharma, A. Dhar, A. Sadiki, Computational investigation of diesel injection strategies in hydrogen-diesel dual fuel engine, Sustain. Energy Technol. Assessments 36 (2019) 100543.

[29] M. Talibi, P. Hellier, R. Morgan, C. Lenartowicz, Hydrogen-diesel fuel co-combustion strategies in light duty and heavy duty CI engines, Int. J. Hydrogen Energy 43 (2018) 9046–9058.

[30] W. Tutak, A. Jamrozik, K. Grab-rogali, Hydrogen effects on combustion stability performance and emissions of diesel engine, Int. J. Hydrogen Energy 45 (2020) 19936–19947.

[31] D.T. Bălănescu, V.M. Homutescu, Effects of hydrogen-enriched methane combustion on latent heat recovery potential and environmental impact of condensing boilers, Appl. Therm. Eng. 197 (2021).

[32] H.W. Wu, T.T. Hsu, J.Y. He, C.M. Fan, Optimal performance and emissions of diesel/hydrogen-rich gas engine varying intake air temperature and EGR ratio, Appl. Therm. Eng. 124 (2017) 381–392.

[33] N. Saravanan, N. Govindan, An experimental investigation on a diesel engine with hydrogen fuel injection in intake manifold, SAE Tech. Pap. (2008).

[34] C. Vipavanich, S. Chuepeng, S. Skullong, Heat release analysis and thermal efficiency of a single cylinder diesel dual fuel engine with gasoline port injection, Case Stud. Therm. Eng. 12 (2018) 143–148.

[35] A. Mejía, M. Leiva, A. Rincón, A. Gonzalez, J. Duarte, Experimental assessment of emissions maps of a single-cylinder compression ignition engine powered by diesel and palm oil biodiesel-diesel fuel blends, Case Stud. Therm. Eng. 19 (100163) (2020) 1–13.

[36] P. Dimitriou, M. Kumar, T. Tsujimura, Y. Suzuki, Combustion and emissions characteristics of a hydrogen-diesel dual-fuel engine, Int. J. Hydrogen Energy 43 (29) (2018) 13605–13617.

[37] P. Dimitriou, T. Tsujimura, Y. Suzuki, Low-load hydrogen-diesel dual-fuel engine operation – a combustion efficiency improvement approach, I Int. J. Hydrogen Energy 44 (31) (2019) 17048–17060.

[38] P. Dimitriou, T. Tsujimura, A review of hydrogen as a compression ignition engine fuel, Int. J. Hydrogen Energy 42 (38) (2017) 24470–24486.

[39] H. Koten, Hydrogen effects on the diesel engine performance and emissions, Int. J. Hydrogen Energy 43 (22) (2018) 10511–10519.

[40] P. Rosha, A. Dhir, S. Mohapatra, Influence of gaseous fuel induction on the various engine characteristics of a dual fuel compression ignition engine: a review, Renew. Sustain. Energy Rev. 82 (2018) 3333–3349.

[41] V. Chintala, K. Subramanian, Experimental investigation of autoignition of hydrogen-air charge in a compression ignition engine under dual-fuel mode, Energy 138 (2017) 197–209.

[42] V. Gnanamoorthi, V. Vimalananth, Effect of hydrogen fuel at higher flow rate under dual fuel mode in CRDI diesel engine, Int. J. Hydrogen Energy 45 (33) (2018) 16874–16889.

[43] P. Sharma, A. Dhar, Effect of hydrogen supplementation on engine performance and emissions, Int. J. Hydrogen Energy 43 (15) (2018) 7570–7580.

[44] V. Chintala, K. Subramanian, A comprehensive review on utilization of hydrogen in a compression ignition engine under dual fuel mode, Renew. Sustain. Energy Rev. 70 (2017) 472–491.

[45] C. Deheri, S. Acharya, D. Thatoi, A. Mohanty, A review on performance of biogas and hydrogen on diesel engine in dual fuel mode, Fuel 260 (2020) 116337.

[46] I. Yilmaz, M. Gumus, Effects of hydrogen addition to the intake air on performance and emissions of common rail diesel engine, Energy 142 (2018) 1104–1113.

[47] A. Jamrozik, K. Grab-Rogaliński, W. Tutak, Hydrogen effects on combustion stability, performance and emission of diesel engine, Int. J. Hydrogen Energy 45 (38) (2020) 19936–19947.

[48] E. Zwolińska, Y. Sun, A.G. Chmielewski, A. Pawelec, Removal of high concentrations of NOx and SO2 from diesel off-gases using a hybrid electron beam technology, Energy Rep. 6 (2020) 952–964.

[49] T. Pi-qiang, Z. Jian-yong, H. Zhi-yuan, L. Di-ming, D. Ai-min, Effects of fuel properties on exhaust emissions from diesel engines, J. Fuel Chem. Technol. 41 (2013) 347–355.

[50] M.A. Rosen, Environmental sustainability tools in the biofuel industry, Biofuel Res. J. 5 (2018) 751–752.

[51] S. Nag, A. Dhar, A. Gupta, Hydrogen-diesel co-combustion characteristics, vibro-acoustics and unregulated emissions in EGR assisted dual fuel engine, Fuel (2022) 307.

[52] C.B. Kumar, D.B. Lata, D. Mahto, Effect of addition of di-tert butyl peroxide (DTBP) on performance and exhaust emissions of dual fuel diesel engine with hydrogen as a secondary fuel, Int. J. Hydrogen Energy 46 (2021) 9595–9612.

[53] M. Karimi, X. Wang, J. Hamilton, M. Negnevitsky, S. Lyden, Status, challenges and opportunities of dual fuel hybrid approaches-a review, Int. J. Hydrogen Energy 46 (2021) 34924–34957.